Surface domain imaging in external magnetic fields

G. Steierl,[a] G. Liu, D. Iorgov, and J. Kirschner
Max-Planck-Institut für Mikrostrukturphysik, Weinberg 2, D-06120 Halle, Germany

(Received 25 February 2002; accepted 22 September 2002)

We report on experimental advances in scanning electron microscopy with polarization analysis that allow the observation of ferromagnetic domains in external magnetic fields of about 0.1 T. This is achieved by using a modified electron optics that produces a magnetic field at the sample surface that is spatially confined on the length scale of 0.1 mm. During imaging, primary and secondary electrons pass through the magnetic field without significant disturbance. We demonstrate that the primary electron beam may be used to keep track of the generated magnetic field. As an exemplary application, the switching processes of rectangular Permalloy elements are analyzed. © *2002 American Institute of Physics.* [DOI: 10.1063/1.1520729]

I. INTRODUCTION

Scanning electron microscopy with polarization analysis (SEMPA) is a well-established technique for the observation of ferromagnetic domains with high resolution and outstanding surface sensitivity.[1–3] These features are at present highly sought, since many industrial applications such as magnetic RAMs and sensors are essentially sub-μm microstructures of ultrathin ferromagnetic films. A drawback of the technique had been that the samples could not be subjected to strong magnetic fields during analysis. Therefore only remanent states could be studied and an analysis of switching processes was impossible unless one resorted to either very weak fields[4] or special samples that could be switched without using magnetic fields within the imaging range. Typically, stray-field free magnetic circuits were investigated, so that the field generating coils could be placed far away from the electron beams used for the measurement.[5] Contrary to these experimental approaches, we investigate in this contribution the possibility of imaging samples that are directly exposed to strong magnetic fields.

In SEMPA [Fig. 1(a)], a well focused high-energy ($\approx$10 keV) electron beam is directed at a surface and the spin-polarization of the ejected low-energy ($\approx$eV) secondary electrons is measured. The spin polarization is known to be directly proportional to the magnetization at the surface,[6] so that the surface domain pattern may be determined. When the sample is exposed to a magnetic field several difficulties may be conceived. First, the spot size of the primary beam could be deteriorated by aberrations. Furthermore, the spin polarization of the secondary electrons could be falsified due to spin precession, and finally, the secondary electron beam could be significantly deflected by the magnetic field, so that the electrons do not reach the spin detector. In the following, it is demonstrated that these difficulties may be suppressed by using a suitable setup.

[a]Electronic mail: steierl@mpi-halle.mpg.de

II. PRINCIPLE OF OPERATION

The main idea behind the approach illustrated in Fig. 1(b) is very simple. All disturbing effects caused by a magnetic field at the sample surface may be reduced by decreasing the transit time through the magnetic field. This is accomplished by using a locally confined magnetic field and an additional electric field to accelerate the slow secondary electrons directly after emission.

In our setup, the magnetic field is confined to a small volume by using a magnetic circuit that ends towards the sample with a narrow gap (pole distance 120 μm) from which the magnetic field protrudes. The sample is positioned close to the magnetic pole pieces (10–40 μm) so that the surface region near the gap can be exposed to strong magnetic fields. The accelerating electric field is generated by placing the magnetic foil and the sample on different potentials, typically several 100 V, depending on the chosen sample to magnet distance. Thus the magnetic pole pieces serve not only as sources of the magnetic field but also as electrostatic electrodes. A subsequent electrostatic quadrupole is used to further accelerate the secondary electrons after passing the gap and to correct for small deflections induced by the magnetic field.

The magnetic circuit was machined from a high permeability foil[7] by using a laser cutter. For precise positioning, the entire assembly is mounted on a three-axes piezodriven positioner. By using the SEM mode the positioning of the magnetic circuit with respect to the sample surface is monitored accurately.

To discuss the performance of the setup it is useful to recall at the outset that the precession of electron spin polarization and the deflection of electrons in a magnetic field are closely related phenomena.[8] This may be seen by examining the equations of motion for the electron velocity $\mathbf{v}$ and the spin-polarization $\mathbf{P}$ in a magnetic field $\mathbf{B}$:

$$m\dot{\mathbf{v}} = e\mathbf{v}\times\mathbf{B}, \quad m\dot{\mathbf{P}} = e\mathbf{P}\times\mathbf{B}, \tag{1}$$

where the approximate gyromagnetic ratio of 2 was used instead of the more accurate value 2.0024. This approximation is completely sufficient in the present context and makes

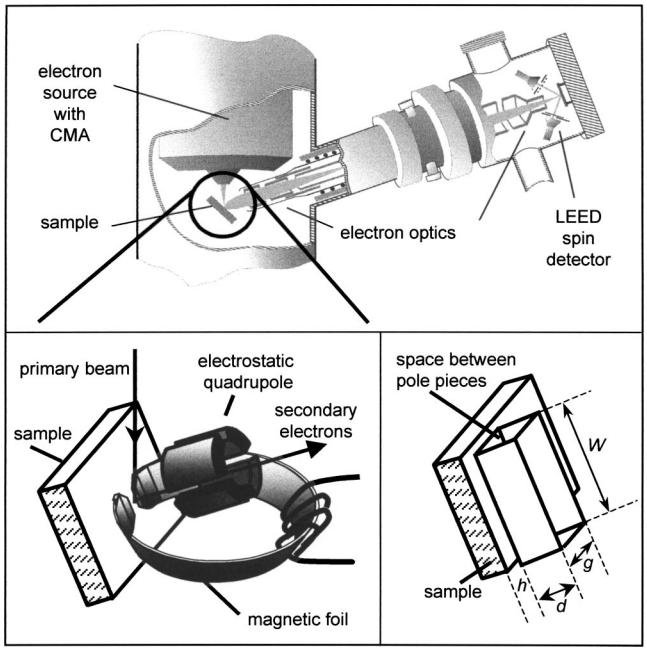

FIG. 1. Basic SEMPA setup (top) consisting of an electron source (PHI SAN 670), electron optics, and a low-energy electron diffraction spin detector. For in-field measurements (bottom left) a miniature magnetic circuit and an electrostatic quadrupole are added to the setup (not shown in scale). Both the primary and secondary electron beam pass through the magnetic gap. The secondary electrons are accelerated by the potentials applied to the sample, the magnetic foil, and the quadrupole. Typical values are: −100 V (sample), ground potential (magnetic foil) and 400 V (electrostatic quadrupole). The volume between the magnetic pole pieces is shown to the bottom right. The adjustable distance between sample and pole pieces (h) is typically chosen between 10 and 40 μm. Further dimensions are: 100 μm magnetic foil thickness (d), 120 μm magnetic gap width (g), and 1 mm magnetic foil width (w). The incidence angle of the primary electron beam used in the experiment is 52° with respect to the sample normal.

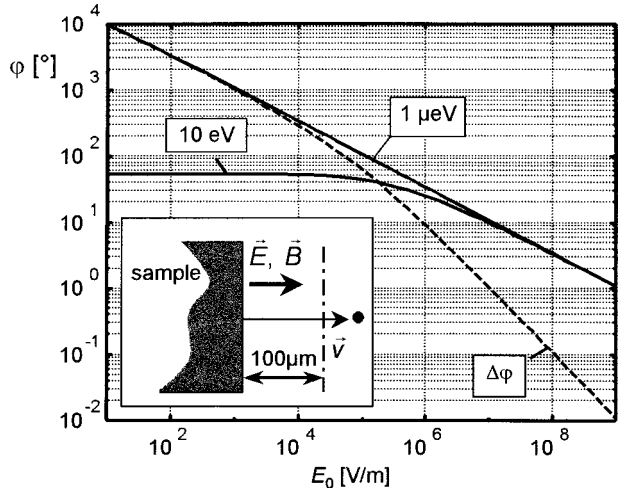

FIG. 2. Precession of spin polarization in homogeneous fields applied perpendicularly to the surface. Shown is the precession angle φ observed at a distance of 100 μm from the surface for electrons emitted with different kinetic energies. The difference of both curves $\Delta\varphi$ is shown as a dashed line. The initial electron velocity is taken to be perpendicular to the surface and the magnetic field strength of 0.1 T is used.

it apparent that both equations of motion are identical. Thus only one solution needs to be considered, which describes the well-known precession of a vector around the direction of the magnetic field. The precession frequency is given by the Larmor frequency ($\omega = geB/2m$), which is independent of vector directions. For a given electron trajectory the time integral over the Larmor frequency may be used to define the total angle of precession φ that is induced by the magnetic field. Since the equations are identical, it is clear that the total precession caused by a magnetic field is the same for the velocity vector and the polarization vector. Therefore, both difficulties associated with secondary electrons, i.e., the bending of the trajectories away from the detector and the precession of spin, can be controlled by considering only a single quantity, the total angle of precession φ. When this value remains small for all detected electrons it is certainly possible to perform meaningful measurements. The dimensions of our setup were chosen to fulfill this requirement, even though it is stricter than absolutely necessary, since one could easily correct for larger values of φ as long as the scatter of φ in the detected electron beam remains small.

For an understanding of the relevant orders of magnitudes it is instructive to discuss the precession in homogeneous fields, even though in reality the fields are inhomogeneous. We therefore assume for the moment, that the electric and magnetic fields are homogeneous within a distance of 0.1 mm from the sample surface, and that the fields are vanishing beyond that distance. Furthermore, the initial velocity of the electrons and the field directions are taken to be perpendicular to the sample surface. The ensuing total precession φ is shown in Fig. 2 as function of the electric field strength and for a magnetic field strength of 0.1 T. The initial electron energies 1 μeV and 10 eV were selected, since these limits cover the secondary electron energy distribution used for spin polarization measurement.

For low electric fields the precession is intolerably large, but above an electric fields strength of about 10^7 V/m, φ becomes tolerably small ($<10°$) and independent of the initial electron energy ($\Delta\varphi < 1°$). At 10^8 V/m even fields of up to 1 T appear to be possible since $\Delta\varphi$ becomes quite small ($\approx 1°$) and φ remains in a regime that could be corrected for by electrostatic deflectors and subsequent data analysis ($\varphi \approx 35°$). The obtainable electric field strength is certainly limited by electric breakdown. Even at flat, polished surfaces under UHV conditions electric breakdown occurs at about 10^9 V/m, since the width of the surface barrier ($\approx$ work function over electric field) becomes comparable to the tunneling length (≈ 1 nm). Our own tests using a miniature magnet machined by laser cutting show that 10^8 V/m may be established after evaporating surface protrusions by sparks, whereas 10^7 V/m can be reached without further ado.

We therefore conclude that spin precession and deflection of secondary electrons can be effectively suppressed in spite of the substantial magnetic field strength of 0.1 T, when the magnetic field is confined to a region close to the surface (0.1 mm) and when a sufficiently large homogeneous electric field is used.

So far, it was assumed that the magnetic field is perpendicular to the sample surface, which is not the case for our setup. However, when φ is small for some perpendicular field strength, it will remain nearly unaltered when the magnetic field is rotated by 90°, since the transit time through the

field is nearly identical for a straight trajectory (perpendicular magnetic field) and a slightly bent trajectory (field in-plane and small value of φ). Thus the above argument remains valid for the geometry used in our setup.

In summary of this section, we have introduced the basic setup and the main idea behind it. The relation of miniaturization, required electric field, and obtainable magnetic field was illustrated by considering a simple order of magnitude estimation. Based on these considerations we have chosen to miniaturize the fields down to about 0.1 mm, which leads to a reduction of the imaging range in the same order of magnitude. This reduction is not a severe drawback for a high resolution microscope, since most microstructures of present day interest are much smaller. In addition, ultrathin films with a lateral size of this dimension are micromagnetically not significantly different from larger samples, since the aspect ratio (thickness over lateral size) is in both cases quite small.

III. PERFORMANCE CHARACTERIZATION BY SIMULATION AND SEM

So far we have highlighted that the two main characteristics of the setup are the beam size of the primary electron beam and the spin-precession angle associated with the secondary electrons. The spin precession angle was discussed for the case of homogeneous fields to establish the validity of the main idea of the present work: the order of magnitude of spin-precession remains small when the fields are localized on the length-scale of about 0.1 mm. Of course, the assumption of homogeneous fields does not allow one to establish an accurate magnetic field limit of the method. In this section, the inhomogeneous electric and magnetic fields are determined by numerical simulation. Then the order of magnitude of spin precession in these realistic fields is discussed.

In the following we do not attempt to provide a complete simulation of the experiment. This would require to work through a fairly large parameter space, since the spin precession in inhomogeneous fields depends on the emission position of the sample and on the initial electron velocity. Furthermore it would be necessary to simulate the primary electron beam spot size as a function of position. This, however, turns out to be a sophisticated problem, since the primary electron beam position on the sample is also sensitive to the far field of the magnet, which leads to the necessity of fairly large data arrays in the simulation. The issue of primary electron beam spot size is therefore not addressed by numerical simulation, but by direct measurement of the spot size. Since most of the spin precession of the secondary electrons takes place within the region of space close to the magnet, it is certainly not a far field problem and truncating the numerical grid is far easier.

A three-dimensional ray tracing program was used for the investigation.[9] For calculating fields close to the center of the gap it is found that the two-dimensional approximation is satisfactory, which might be expected from the large aspect ratio of the pole pieces ($g/w=10$). As a boundary condition for magnetic field calculation constant magnetic potentials on the surfaces of the pole pieces were used. This is applicable due to the high permeability of the magnetic material ($>25\,000$).[7]

The magnetic field produced by the magnetic circuit is in general not only given by the excitation current of the magnetic circuit, but also depends on the magnetic sample. The influence of the sample may be quantified by using the method of image charges. When a thick sheet of high permeability material (a magnetic head as shown in Fig. 1 but without the gap) is brought close to a thin film material the magnetic charges of the film are perfectly mirrored at the head surface closest to the thin film. When the head is positioned very close to the surface (closest approach is 10 μm), the mirror charges appear at a distance of 20 μm above the surface, which is still much larger than the typical thin film thickness ($\sim$10 nm). This geometry results in very small fields due to the mirror charge, as can be seen by considering the worst case of a straight 180° head on wall that extends throughout a film. The mirror charge is much further away than the film thickness or the typical wall width so that the mirror charge field can be calculated by using a line charge with constant density. With a saturation magnetization of 2 T and a film thickness of 10 nm, the maximum field at the sample surface due to the mirror charge becomes 3.2 Oe and at the peak position, the mirror charge field is perpendicular to the film. Considering that such weak fields result from a worst case consideration one may expect that mirror charges are completely negligible for most ultrathin film systems.

This also holds for the investigation of thin microstructures, as can be easily seen by noting that the mirroring surfaces tend to be further away since the distance to the magnetic head is decisive. For example, for a completely saturated microstructure of lateral dimension $20\times 20\ \mu\text{m}^2$ positioned in the middle of the gap, the field generated by the mirror charges is 0.18 Oe in the middle of the gap, where we assumed a saturation magnetization of 2 T, a thickness of 100 nm, and a head consisting of two perfect mirror planes (i.e., infinite foil thickness d in Fig. 1). Therefore the magnetic field produced by the magnetic circuit is calculated without including a magnetic sample. Nonetheless, it should be noted that this reasoning will break down when films or microstructures with a thickness of several μm are investigated.

The result for the magnetic field in the plane of the surface is shown in Fig. 3. The field strength is normalized to the field (B_0) given by the ratio of the magnetostatic potential drop across the gap and the gap distance. This is identical to the average field along a line connecting the centers of the pole pieces. The in-plane field is very homogeneous over a large fraction of the pole piece distance. In addition, the magnetic field does not drop steeply with increasing distance between sample and magnet, e.g., for 10 and 40 μm distance the field at the sample surface and in the middle of the gap is about 0.8 and 0.6 B_0, respectively.

However, the magnetic field is not completely in the plane of the surface. Since the perpendicular component vanishes in the antisymmetry plane its relative importance depends mainly on the size of the imaging range. For scan ranges that do not deviate from the antisymmetry plane by more than about 5 μm, the perpendicular component amounts to only a few percent of the in-plane field. It should

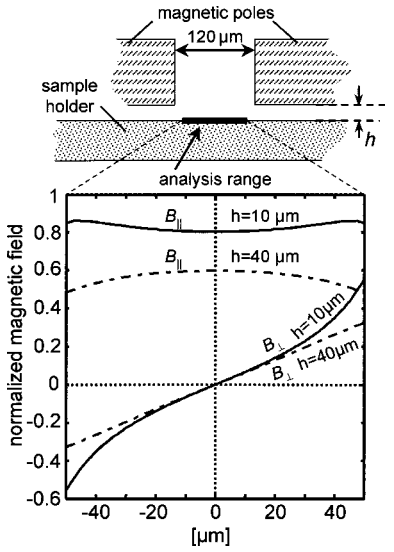

FIG. 3. In-plane ($B_{\parallel}$) and out-of plane ($B_{\perp}$) field components in the analysis range of 100 μm for different distances (h) of 10 and 40 μm between magnetic pole pieces and sample surface. The magnetic field is normalized to the average field B_0.

be noted that in-plane fields are applied to investigate ultrathin systems with in-plane easy axes. In most cases, the weak perpendicular component is very unlikely to have an effect on these systems.

A ray tracing simulation was performed to investigate the trajectories of secondary electrons. Again, the two-dimensional approximation turned out to give accurate results for electrons starting near the center of gap, since most of the spin precession takes place when the electrons are slow and the fields are strong, i.e., in the region close to the sample surface. Due to that the fields were truncated at a distance of 0.6 mm from the sample surface. For simplicity the electrostatic quadrupole shown in Fig. 1 was omitted which leads to a slight overestimate of the precession angle.

The main feature found by simulation may be understood by considering the electric field. In the present design, the accelerating field at the sample surface and in the middle of the gap E' is smaller than the field inferred from the potential drop U and the distance h between sample and magnet ($E_0 = U/h$). For example, for a sample to magnet distance of 40 μm, E' is about 55% of E_0. In addition, the accelerating electric field decreases rapidly with increasing distance from the sample surface. These two effects lead to a reduction of the acceleration and therefore to an increase of spin precession compared to the homogeneous field approximation discussed in the context of Fig. 2. To guarantee that φ remains below 30° for electrons starting perpendicularly along the central axes of the setup, we find from the ray tracing simulation that E_0 must be 10^7 V/m for a magnetic field at the sample surface of 0.1 T and a sample to magnet distance of 40 μm. For the same fields the homogeneous field approximation yields a spin precession of about 10°, which is smaller but not substantially different. Thus the important order of magnitude of the achievable magnet field inferred from Fig. 2 is corroborated by the ray tracing simulation.

Since the electric field is limited, progress towards higher magnetic fields could be accomplished by further decreasing the overall size of the setup while keeping the geometric arrangement unaltered. When considering secondary electrons with vanishing initial energy the precession angle φ becomes proportional to the factor $\sqrt{dB_0^2/E_0}$, where d may be an arbitrary chosen length (e.g., the magnetic foil width) and B_0 and E_0 may be defined in the way given above. This rule follows directly from the scaling properties of the nonrelativistic ray equations.[10] When the setup is scaled down by some factor of k, i.e., $d' = d/k$, the magnetic field strength that yields the same precession angle φ will of course increase, but only by a factor of $\sqrt{k}$. Here, we assumed that E_0 remains unaltered when scaling the overall size of the setup, which is reasonable, since in any case, one will attempt to operate the electric field at a fixed value close to electric breakdown. In total we see that progress towards higher obtainable magnetic fields by scaling the setup is rather slow due to the linear dependence of φ on B_0 and the square root dependence of φ on the overall length scale d. It should be emphasized that up to now we required that all secondary electrons including those with vanishing initial energy pass the magnetic field without significant spin precession. For very small dimensions, e.g., $k = 100$, this requirement appears to be overly stringent, since a large fraction of the secondary electrons has sufficient initial energy to pass the magnetic field even without being accelerated by an electric field. This may be easily seen by noting that the typical energy of 1 eV leads to a radius of curvature of 3.4 μm when a field of 1 T is applied perpendicular to the electron velocity. Thus, towards smaller dimensions, one may expect progress beyond the scaling limit introduced above because the typical energy of the secondary electrons becomes important.

Care must be taken when the scaling argument is used to design setups with a larger range of view, i.e., larger pole piece distance, at the expense of lower obtainable magnetic fields. When the ratio $\sqrt{dB_0^2/E_0}$ is kept constant the situation remains essentially unaltered as regards to the secondary electron beam, but in such an up-scaling attempt, the primary beam properties are quickly aggravated due to the increase of field induced aberrations.

To investigate whether aberrations decrease the obtainable resolution we studied the dependence of the primary electron spot size on the magnetic field. This is achieved by using SEM mode, since it is much easier to accurately measure the primary electron beam spot size by SEM line scans than by SEMPA line scans. As the sample a square grid with a periodicity of 25 μm is used. Large scale SEM images (100×70 μm^2) of the sample are shown in the insets of Fig. 4. Both images in the top and bottom panel are recorded with identical settings of the primary electron beam column (20 kV beam energy, 1 nA current). The visible shift of the field of view is caused by the deflection of the primary electron beam in the magnetic field. It is remarkable that no sizeable distortion of the grid is observed, though the scan range of 100 μm in the horizontal direction covers most of the field of view between the pole pieces (120 μm pole-piece distance).

The displayed line scans are recorded at the edge of the grid using the highest magnification (500 000) and with the primary beam in the symmetry plane of the gap. The same

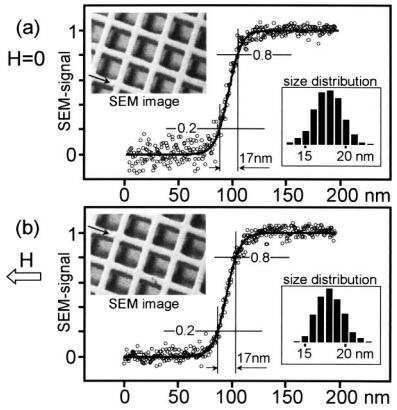

FIG. 4. Influence of the magnetic field on SEM imaging and SEM resolution. In the top panel the magnetic field is turned off and in the bottom panel a field of 32 mT is applied. The insets towards the left display SEM images ($100\times70\ \mu m^2$) of the sample. With respect to these images the applied field direction is horizontal. A small irregularity of the grid is marked by arrows. The shift of the field of view due to the magnetic field by about 40 μm towards the vertical direction is visible by comparing the position of the irregularity in both images. The displayed line scans are recorded with optimized astigmator settings at the edge of the grid using highest magnification. From the normalized line profiles the 20/80 beam size is found from the distance of the corresponding level crossings at 0.2 and 0.8. To facilitate the detection of the level crossing the line profiles are fitted by an error function. A histogram of the beam size distribution inferred from evaluating 250 line scans is shown in the bottom insets. The good agreement of both distributions shows that there is no significant loss of resolution due to the magnetic field.

beam parameters are used for both measurements except that focus and astigmator settings are optimized each time since the optimal setting depends on the magnetic field strength. From the normalized line profiles the 20/80 beam size is found from the distance of the corresponding level crossings. To facilitate the detection of the level crossing the line profiles are fitted by using an error function. The beam size determined from the displayed line scans are identical (17 nm). Thus no resolution loss is apparent for the magnetic field strength used in the measurement (32 mT at the sample surface). Considering that the line scans are recorded slightly below the regular working distance (by about 3 mm) the obtained beam sizes of 17 nm agree to the specification of the electron source manufacturer, who guarantees a beam size of 15 nm at working distance.[11]

Since comparison of single line scans may be misleading due to the scattering of the signal we determined the beam size distribution by evaluating in both cases 250 lines (bottom insets). Both distributions agree within an error below 2 nm. From the evaluation of several size distributions it is found that the reproducibility of beam size measurement is about 2 nm. This limit stems from the fact that the measurements with and without magnetic field should be performed on the same position of the sample and for each measurement the focus and astigmator setting has to be optimized. Thus deviations below about 2 nm cannot be reliably detected or attributed to the magnetic field. Within these limits, the results, however, clearly demonstrate that there is no resolution loss due to the magnetic field.

In summary, we have detailed the characteristics of the setup. It was shown that the spin precession due to realistic inhomogeneous fields is of the same order of magnitude as expected from the homogeneous field approximation. Therefore this should not limit the method up to fairly strong fields of about 0.1 T. As regards to the primary electron beam spot size, it was demonstrated that no resolution loss can be detected up to fields of 32 mT. We emphasize that both considerations did not probe the entire parameter space since we restricted the discussion to electron beams in the symmetry plane of the setup. Naturally, the performance test that includes the entire setup is direct magnetic microscopy, which is the subsequent topic.

IV. IN-FIELD MAGNETIC MICROSCOPY

As an exemplary application, we report in the following on the switching behavior of Permalloy microstructures ($Ni_{80}Fe_{20}$, 50 nm thick). These were produced in a variety of sizes and shapes by electron-beam lithography and lift-off. As the substrate a Si(111) wafer with a natural oxide layer was selected, since the commonly used thermally oxidized Si wafers usually give rise to charging effects. For protection against oxidization during transport the microstructures were covered by a cap layer (Cu, 2 nm thick). This layer was subsequently removed by *in situ* Ar-ion bombardment (3 kV, 60° with respect to the sample normal). During sputtering Auger electron spectroscopy (AES) was used to monitor the chemical composition at the surface.

For in-field measurements the demagnetized magnetic circuit was inserted and positioned close to the sample surface (35 μm). The positioning was directly monitored by using the SEM mode. As primary beam energy 15 kV was chosen. During imaging it is found that focus and astigmators have to be readjusted after changes of the magnetic field. Using a properly adjusted primary beam of 10 nA with a spot size below 30 nm no deterioration of resolution due to the magnetic field is detected in the SEM mode. However, we find by using AES that the presence of the magnetic circuit decreases the time that the surface remains clean. Mainly carbon is detected shortly after inserting the magnetic circuit, which might be caused by electron induced desorbtion from the magnetic circuit. The carbon contamination decreases the spin polarization and therefore prolongs the necessary data-acquisition time in SEMPA measurements. The reduced signal and the prolonged measurement time lead to a slight decrease of resolution in the subsequent SEMPA measurements.

As demonstrated above (Fig. 4), the magnetic field acts as a deflection unit on the primary beam. For the primary beam energy and the sample–magnet distance chosen, it is found that the scan range shifts on the sample surface by the amount of 1.9 μm/mT. This value was determined by using a calibration sample, as explained in more detail elsewhere. It is important to note that the shift of the primary beam position is experimentally extremely helpful, since it allows for direct measure of the magnetic field strength. For example, to reproduce a certain field value, the excitation coils of the circuit are simply set to the value that reproduces the previously recorded primary beam position. The small hysteresis of the magnetic circuit, that is encountered, causes no prac-

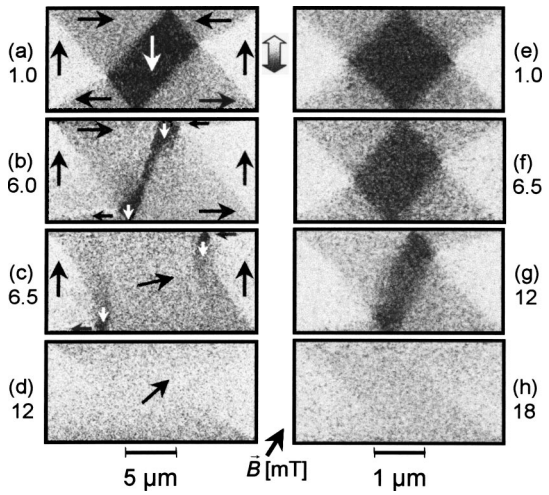

FIG. 5. Switching processes of Permalloy rectangles (50 nm thick) with lateral dimensions $20\times10\ \mu m^2$ (left column) and $4\times2\ \mu m^2$ (right column). The images display the in-plane spin polarization component in the up-down direction, as indicated by the shaded arrow. The magnetization directions given by the arrows within the images follow from the combination of both measured in-plane components. For simplicity, only one component is shown here. The switching processes (a)–(d) and (e)–(h) were observed by increasing the field from zero in the direction given by the arrow at the bottom. Both elements were on the same substrate so that the elements could be imaged sequentially in the same field. The field strength is given to the left and right in mT.

tical problems, since the magnetic field is determined by primary beam position and not by reference to the current to field relationship of the magnetic circuit.

The switching processes of rectangular microstructures are shown in Fig. 5. Rectangles were investigated since this shape has been investigated previously by several groups.[12–15] Starting from the remanent state the magnetic field is applied under 60° with respect to the long axis of the rectangle. This field favors the domains in the top-left and the bottom-right corner. Consequently these domains expand with increasing field at the expense of the other three domains. Especially the domain in the center shrinks rapidly with increasing field. At a field of 6 mT [Fig. 5(c)] the domain in the center is so narrow that a slight increase of the field leads to a modification of the entire domain structure [Fig. 5(d)]. After the collapse of the domain in the center two vortices remain close to the upper and lower edge. With further increase of the field the vortices are driven towards the edges and finally disappear [Fig. 5(e)]. In smaller rectangles essentially the same switching process is observed, though the required fields for saturation are found to be larger. A domain structure with two vortices, as shown in Fig. 5(c), was not encountered in smaller microstructures, though this might be simply due to the large steps that were used to increase the field strength.

The observed switching process agrees qualitatively with micromagnetic calculations,[15] even though the sizes and field directions considered in the calculation are quite different. Most importantly, the results clearly show that SEMPA measurements in strong magnetic fields can be accomplished. So far, 32 mT were the largest fields that could be produced by the present setup. Larger fields were not applied due to limitations of the excitation current caused by overheating and due to flux leakage of the magnetic circuit. Up to the maximum field of 32 mT no losses of spin signal or SEM resolution were detected, which indicates that the field strength limit for in-field SEMPA measurements should be encountered at considerably larger fields.

V. DISCUSSION

We investigate the simple idea that locally confined magnetic fields combined with strong electric fields could allow for the direct observation of switching processes by SEMPA. Since this leads to a decrease of the field of view, this method is particularly well suited for the investigation of microstructured samples with a lateral size below about 50 μm. For larger samples, e.g., ''infinite'' ultrathin films, the magnetization loop observed with the localized magnetic field may differ from the loop observed in macroscopic fields, depending, for example, on the nucleation processes of the film. To investigate ultrathin films, it is advantageous to produce structured samples, since from a micromagnetic point of view, real ultrathin films are always microstructures with large length to thickness ratio and this is also the case when nm thick films are structured to sizes of about 50 μm.

As regards to the setup we have highlighted the main characteristics. This clearly demonstrates that there is ample opportunity to design in-field SEMPA setups, contrary to the long prevailing conviction. A particularly simple design is realized and used to investigate the switching processes of Permalloy elements. The results show unambiguously and for the first time that SEMPA measurements in strong magnetic fields can be performed.

ACKNOWLEDGMENTS

The authors thank Wim Lutzke and Hans Peter Oepen for fruitful discussions and for providing essential parts of the instrumentation. The authors also wish to thank Claus Schneider and coworkers at the IFW-Dresden for preparing the sample.

[1] K. Koike and K. Hayakawa, Jpn. J. Appl. Phys., Part 2 **23**, L187 (1984).
[2] H. P. Oepen and J. Kirschner, Scanning Microsc. **5**, 1 (1991).
[3] M. R. Scheinfein, J. Unguris, M. H. Kelley, D. T. Pierce, and R. J. Celotta, Rev. Sci. Instrum. **61**, 2501 (1990).
[4] R. Allenspach, IBM J. Res. Dev. **44**, 553 (2000).
[5] A. Gavrin and J. Unguris, J. Magn. Magn. Mater. **213**, 95 (2000).
[6] J. Kirschner, in *Surface and Interface Characterization by Electron Optical Methods*, edited by A. Howie and U. Valdré (Plenum, New York, 1988), p. 267.
[7] The magnetic foil is available from Magnetic Shield Corporation (Bensenville, IL) under the trademark CO-NETIC AA.
[8] J. Kessler, *Polarized Electrons*, 2nd ed. (Springer, Berlin, 1983).
[9] The program SIMION 3D 6.0 available from Princeton Electronic Systems, Inc. was used for field calculation and ray tracing simulation.
[10] M. Szilagyi, *Electron and Ion Optics* (Plenum, New York, 1988), pp. 47–50.
[11] Specification of the scanning Auger nanoprobe 670 available from Perkin Elmer Inc., Physical Electronics Devision, 1991.
[12] B. W. Corb, IEEE Trans. Magn. **24**, 2386 (1988).
[13] S. McVitie and J. N. Chapman, IEEE Trans. Magn. **24**, 1778 (1988); Microsc. Microanal. **3**, 146 (1997).
[14] J. G. Zhu, Y. Zheng, and X. Liu, J. Appl. Phys. **81**, 4336 (1997).
[15] R. Hertel and H. Kronmüller, Physica B **275**, 1 (2000).